1998

Interfacial fracture toughness and the role of moisture in microelectronic packaging materials

Ryan M. Hydro
Lehigh University

Hydro, Ryan M.

Interfacial Fracture Toughness and the Role of Moisture...

January 11, 1998

Interfacial Fracture Toughness and the Role of Moisture in Microelectronic Packaging Materials.

By: Ryan M. Hydro

A Thesis

Presented to the Graduate and Research Committee

of Lehigh University

in Candidacy for the Degree of

Master of Science

in

Materials Science and Engineering

Lehigh University

September 1997

CERTIFICATE OF APPROVAL

This thesis is accepted and approved in partial fulfillment of the requirements for the Master of Science in Materials Science and Engineering.

11/25/97
Date

Raymond A. Pearson
Thesis Advisor

Chairman of Department

ACKNOWLEGMENTS

I would sincerely like to thank my advisor, Professor Raymond Pearson, for giving me the opportunity to pursue my masters degree at Lehigh University. He gave much of his time and effort during the past two years in helping me to become a better scientist and researcher.

The help of Dr. Reza Bagheri, who's stay was cut short due to unfortunate circumstances, at the onset of my research as well as the help of Malcolm Early is appreciated.

Thanks to all the support staff in the Mat Sci & Eng Dept, in particular, Carol, Pat, Maxine, and Virginia. I would also like to thank Gene and Arlan for their help, especially, in dealing with the Mechanical Behavior Laboratories.

Funding through the Semiconductor Research Corporation Grant #PJ-554-95 is greatly appreciated. The materials supplied for this research from Ablestik, Dexter, Epoxy Technology, IBM, Olin Corporation, and TI are appreciated.

Finally, but most importantly, I would like to thank my parents, Ronald and Maryanne, and my sister, Erin, for all the love and support (both emotional and financial) they have given me over the years. I couldn't have made it this far without them. Also, I would like to take this moment to thank my mother for giving me her ability to break things. The only difference is that I actually break things on purpose!!!!!!!!

TABLE OF CONTENTS

LIST OF TABLES

LIST OF FIGURES

ABSTRACT

Recently, the microelectronics industry has been shifting its resources away from conventional ceramic packaging and towards plastic packaging. The advantages of plastic packages are lower overall package weight and cost. Silver-filled adhesives are typically used in the microelectronics industry to bond silicon integrated circuit chips to a wide variety of substrates. The substrates include copper, silver, nickel/palladium, polyimide, and glass-filled epoxies. This work will examine the adhesive strength of several silver-filled epoxy die-attach adhesives on copper leadframe substrates. Specifically, H35-175MP (Epo-Tek), AB84-1LMISR4 (Ablestik), and KO111 (Dexter) die-attach adhesives will be examined on Olin C-194 Cu alloy and on a Ni/Pd coated C-194 Cu alloy. In order to quantify the adhesive strength, the interfacial fracture toughness will be determined through the use of the mixed-mode bending test (MMB).

The adhesive strength of each system will be determined under ambient conditions as well as after a conditioning of 85°C/85% RH for 168 hours. In addition, the Olin C-194 Cu alloy will be cleaned with UV ozone for 0, 5, and 10 minutes in order to determine the effect of cleaning on adhesion. It was found that adhesion in these systems significantly decreased upon exposure to an elevated temperature and humidity conditioning of 85°C/85% RH for 168 hours when compared with ambient. Also, UV ozone cleaning of the C-194 Cu alloy was not found to influence the adhesive strength.

1. INTRODUCTION

The field of microelectronics packaging is one that is rapidly evolving. Each microelectronics package consists of many components, all of which must function properly and efficiently, for the projected lifetime of the package. Recently, the microelectronics industry has been shifting its resources away from conventional ceramic packaging and applying more resources towards plastic packaging. Failure may occur at any one of a number of interfaces located within a typical plastic package. The projected lifetime of plastic packages can be related to interfacial failure. Typically, the interfaces are either metal—polymer or ceramic—polymer in nature. At any point within the plastic package where a bimaterial interface exists, the opportunity for fracture is increased, due to elastic moduli and coefficient of thermal expansion (CTE) mismatches. Failure is also intensified when packages are exposed to external stresses such as temperature and humidity during package processing and customer usage. Of utmost importance in these packages is the interfacial fracture strength or in other words the amount of adhesion at each interface.

Therefore, this study will examine the interfacial fracture toughness of microelectronics packaging materials and relate these mechanical measurements of adhesion to the thermodynamic work of adhesion. Three silver-filled epoxy die-attach adhesives will be examined on various substrates both with and without the presence of moisture.

1.1 Fracture Mechanics

The fracture behavior of a material is very important in designing engineering structures or components subjected to stresses. Understanding the fracture behavior of a material under an applied load in the presence of a defect or flaw is of great significance. Depending on the magnitude of the load and its point of application, as well as on the size of the flaw (crack) present, a material can behave in a number of ways. A. A. Griffith[1] developed the first fracture criterion, which was based primarily on an energetic criterion. Griffith's fracture criterion balances the decrease in potential energy associated with movement of the applied loads and the increase in surface energy due to crack formation[2].

For an infinitely wide plate as shown in Figure 1, containing a central crack of total length 2a, Griffith developed an equation for the change in potential energy of the plate associated with crack introduction. This relation is found in Equation 1.1 below:

$$U - U_o = -\frac{\pi \sigma^2 a^2 t}{E} + 4at\gamma_s \qquad [1.1]$$

where,

U = the potential energy of the body with a crack

U_o = potential energy of the body without a crack

σ = the applied stress

a = the half-crack length

t = the plate thickness

E = modulus of elasticity

γ_s = the specific surface energy

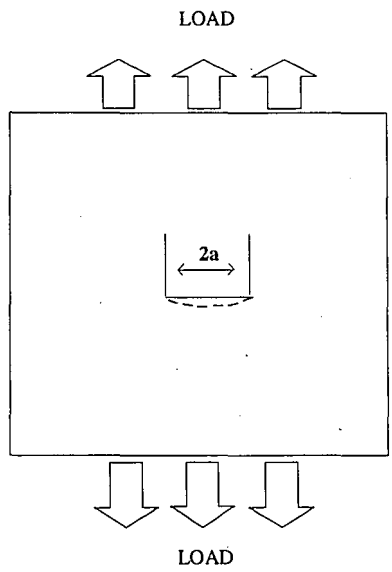

Figure 1. An infinitely wide plate, containing a central crack of total length, 2a.

By rearranging Equation [1.2], and taking $\partial U/\partial a$ and setting the result equal to zero, one obtains the equilibrium condition, which is finally found in Equation [1.3] below:

$$\frac{\partial U}{\partial a} = 4t\gamma_s - \frac{2\pi\sigma^2 at}{E} = 0 \qquad [1.2]$$

Therefore,

$$2\gamma_s = \frac{\pi\sigma^2 a}{E} \qquad [1.3]$$

In order to quantify the distribution of the stresses located at a crack tip in a material, Irwin[3], developed a variable termed the stress intensity factor, K. The value of K, depends on the structural geometry, the applied load, and the crack length present in the material. Equation [1.4], shows the relation for calculating the stress intensity factor, K.

$$K = Y \sigma \sqrt{a} \qquad [1.4]$$

where,

K is the stress intensity factor, Y is the geometric factor[4], and a is the half-flaw length.

Once K reaches a critical value, termed K_c, fracture occurs. K_c is termed the fracture toughness or critical stress intensity factor of the material. The fracture toughness is a measure of a material's resistance to fracture in the presence of a flaw/crack, when subjected to an applied load.

Two common types of loading conditions occur based upon the thickness of the material being subjected to the applied load. These are termed plane stress (thin sheets) and plane strain (thick sheets) behavior. Equations [1.5] and [1.6] are for calculating the fracture energy for plane stress and for plane strain conditions, respectively[5]. A plane stress is associated with a biaxial stress state at the crack tip, whereas a plane strain condition is associated with a triaxial stress state at the crack tip.

$$G=\frac{K^2}{E} \qquad \text{(plane stress)} \qquad [1.5]$$

$$G=\frac{K^2}{E}(1-\nu^2) \qquad \text{(plane strain)} \qquad [1.6]$$

where,

G is the strain energy release rate, K is the stress intensity factor, E is the elastic modulus, and ν is Poisson's ratio.

At fracture, the strain energy release rate, G, reaches a critical value, G_c. This value is termed the critical strain energy release rate. The loading Modes are depicted in Figure 2. Mode I, is the pure tensile or crack opening component of the load, Mode II, is the in-

plane shear component, and Mode III, is the out-of-plane shear or torsional component of the applied load.

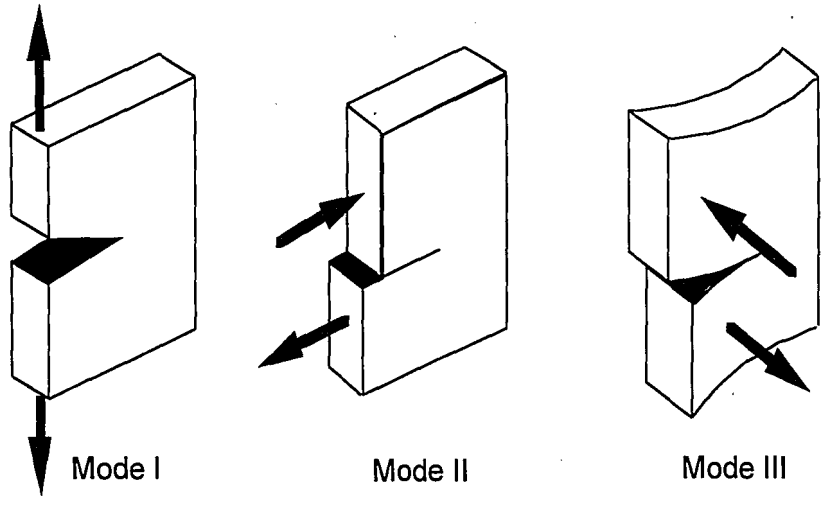

Figure 2. Schematic diagram depicting pure tensile (Mode I), in-plane shear (Mode II), and out-of-plane torsion (Mode III) types of crack loading modes (from Hertzberg[5]).

1.2 Mode-Mixity

The majority of failures occurring at interfaces in microelectronic packages are mixed in nature, ie. the materials fail due to a combination of Mode I and Mode II types of loading. Charalambides and Kinloch et al.[6] have examined mixed-mode fracture behavior by utilizing two different approaches, namely, the local and global methods. The local method is concerned with the local singular field ahead of the crack tip, whereas, the global approach is concerned with applied energy release rates. In analyzing the mixed-mode fracture behavior with the global approach, one partitions the total strain energy release rate, G_T, into both its crack opening mode (mode I), G_I, and its sliding mode (mode II), G_{II}. The mixity of the system as defined by Hutchinson[7] is then simply the ratio of mode II to mode I behavior as shown in Equation [1.7].

$$\mathrm{Tan}^2(\psi) = \frac{G_{II}}{G_I} \qquad [1.7]$$

where,

ψ is the mixity angle, G_{II} the strain energy release rate due to mode II type loading, and G_I is the strain energy release rate due to mode I type loading.

A significant amount of research has been accomplished on pure-Mode I (DCB) and on pure Mode II (ENF) types of loading. Charalambides and Kinloch et al.[6] have analyzed mixed mode failures using both a local and global approach to the interfacial fracture energy. They have taken both Mode I and II types of loading into consideration and have shown that the global approach to the interfacial fracture energy gives better agreement between theoretical calculations and experimental results for interlaminar fracture. Charalambides and Kinloch et al.[6] favor the global approach over the local approach, since the local approach uses a very localized singular dominated region ahead of the crack tip, it possesses a large damage zone, and surface roughness interactions would tend to obscure the singularity. Finally, the authors have developed a criterion, Equation [1.8], for fracture behavior under mixed-mode loading conditions.

$$G_o = G_c [\cos^2 (\psi - \psi_o) + \sin^2(\omega) \sin^2 (\psi - \psi_o)] \qquad [1.8]$$

where,

G_c is the measured critical strain energy release rate, ψ is the phase angle of the applied loads, ψ_o is the phase angle due to elastic mismatch across the bimaterial interface, and ω is the slope of the fracture surface roughness.

A valuable tool for evaluating this mixed-mode loading behavior at bimaterial interfaces is the Mixed Mode Bending Test (MMB) which was originally developed by Reeder and Crews[8,9] to study interlaminar failure in composites. A schematic of their test fixture can be found in Figure 3. The advantage of using the MMB test fixture is that it enables one to apply any loading mixity between a pure Mode I (double cantilever beam) and a pure Mode II (edge-notch flexural) test. Therefore, the mixity angle can be varied from 0 to 90 degrees. The types of failures observed can be either cohesive or adhesive in nature. By employing a mixity angle of 46°, ie. equal contributions of Mode I and II loading, interfacial or adhesive failure is ensured.

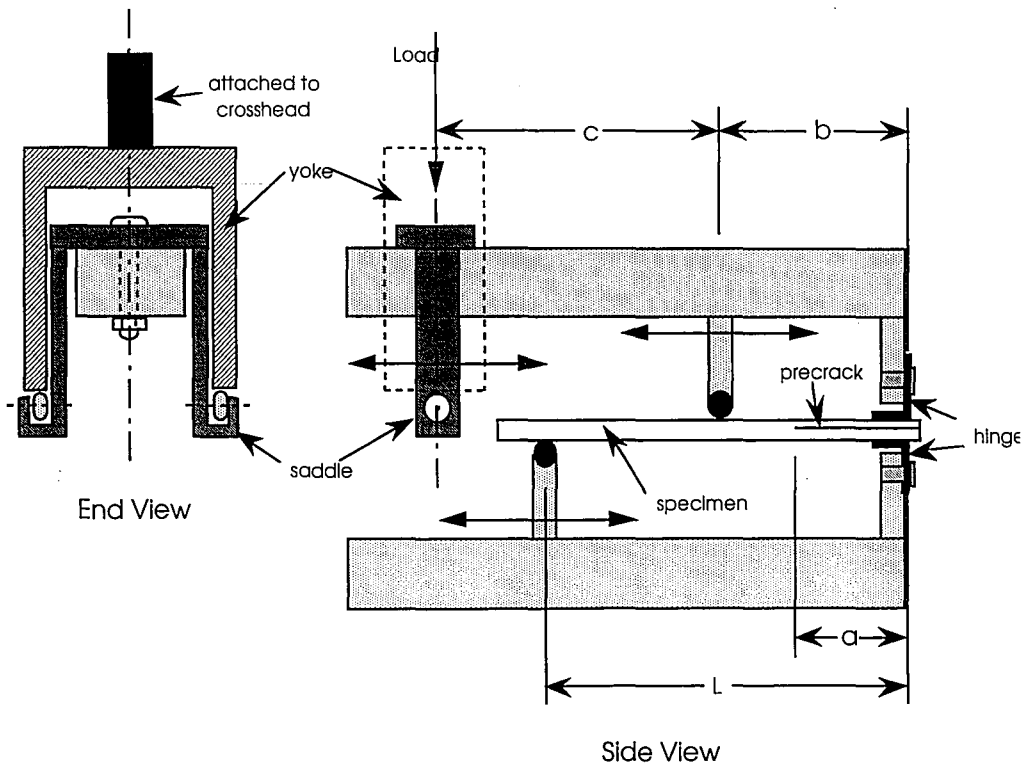

Figure 3. Schematic Diagram of Mixed-Mode Bending (MMB) Fixture (from Brandenburger[10]).

Equations [1.9] and [1.10], are the equations used in order to calculate the G_{IC} and G_{IIC} interfacial fracture energies for the MMB test fixture.

$$G_{IC} = \frac{3P^2 (a + \chi_I h)^2}{B^2 E_{11} h^3} \left[(1 - \frac{c + b}{L})F_2 - \frac{c}{b} F_1\right]^2 \qquad [1.9]$$

$$G_{IIC} = \frac{9P^2 (a + \chi_{II} h)^2}{4B^2 E_{11} h^3} \left[(1 - \frac{c + b}{L})F_2 + \frac{c}{b} F_1\right]^2 \qquad [1.10]$$

where,

b, c, and L are fixture parameters (m), see Figure 3.

a, is the initial crack length from the center loading point of the center hinge position to the corresponding crack tip (m).

χ_I and χ_{II}, are correction factors for Mode I and Mode II, respectively.

h, is the half-thickness of the specimen (m).

F_1 and F_2, are correction factors due to the large deflection of the loading arms.

This angle of mixity can be varied through variation of the fixture parameters b, c, and L (Figure 3). The contributions to the interfacial fracture energy due to both Mode I and Mode II loading can then be separated out. Through addition of the G_{IC} and G_{IIC} components of the interfacial fracture energy, a global interfacial fracture energy, $G_{I/IIC}$, can be determined as in Equation [1.11], shown below:

$$G_{I/IIC} = G_{IC} + G_{IIC} \qquad [1.11]$$

where,

$G_{I/IIC}$ is the global interfacial fracture energy (J/m^2).

G_{IC} is the interfacial fracture energy due to Mode I (J/m^2).

G_{IIC} is the interfacial fracture energy due to Mode II (J/m^2).

1.3 MMB Testing

Previous Mixed-Mode Bending studies have been conducted by Brandenburger[10] and Early[11]. Brandenburger[10] has examined the mixed-mode fracture behavior of two filled-epoxy die-attach adhesives using the Mixed-Mode Bending Fixture. The author observed that the thickness of the adhesive bondline, significantly affects the value of the interfacial fracture energy. Brandenburger also found that reproducible adhesive failure occurred when a mixity angle of 46° was utilized. Early[11] examined the mixed-mode fracture behavior of ten different organic die-attach adhesives on both FR-4 and IBM Cu foil substrates using the Mixed-Mode Bending Fixture. A reasonable correlation

between the interfacial fracture energy and the thermodynamic work of adhesion for adhesive failure was found to exist.

1.4 Adhesion

Adhesion can be defined as the ability of a polymeric material to join two dissimilar surfaces together in a stable manner. The bond between adhesives and substrates in microelectronic packaging is of paramount importance. The adhesive needs to wet the area of contact and then flow or spread over the entire surface area in order to join the two materials together and provide a strong and reliable joint. Many factors exist which affect the adhesive strength between two materials. Among them are the cleanliness of the substrate, moduli, coefficients of thermal expansion, the polarity of the substrate and adhesive, and finally the viscosity and porosity of the adhesive. The thermal history of the joint as well as moisture exposure can have a significant affect of the reliability of the bound joint. Nguyen et al. [12,13] has shown that both temperature and moisture exposure can significantly affect the mechanical and electrical reliability of microelectronic package configurations.

In order to characterize the ability of a given adhesive to wet or spread over a given surface, the contact angle method is most frequently utilized. The contact angle method measures the angle of contact between a surface and a liquid which is deposited on the substrate's surface. A typical contact angle experiment is shown in Figure 4. The

sessile drop of liquid is deposited on the substrate's surface and the angle of contact between the liquid and substrate is measured. This method of contact angle measurement can be attributed to the "father of wettability studies", Young[14]. The equation developed for the angle of contact can be found in Equation [1.12] below:

$$\gamma_{SV} = \gamma_{SL} + \gamma_{LV} \cos\theta \qquad [1.12]$$

where,

γ_{SV} is the surface tension between the solid and vapor, γ_{SL} is between the solid and liquid, and $\gamma_{LV} \cos\theta$ is the surface tension between the liquid and vapor multiplied by the contact angle.

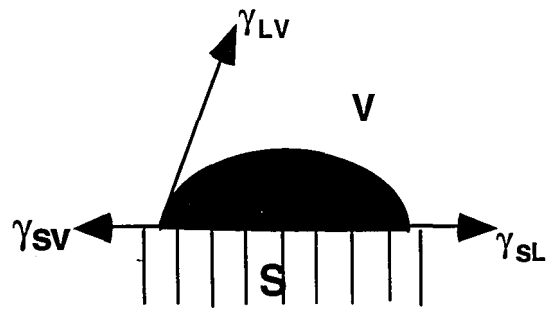

Figure 4. Method of Contact Angle Measurement. Diagram shows the liquid deposited on the surface of the substrate.

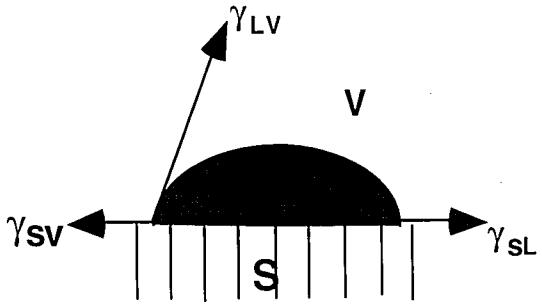

Figure 4. Method of Contact Angle Measurement. Diagram shows the liquid deposited on the surface of the substrate.

For the spreading of a liquid over a substrate, there are three surface free energies associated with the process. In order for the spreading of the liquid to be spontaneous, the process must be energetically favorable. The energetics associated with the spreading process are governed by Equation [1.13] below:

$$\gamma_{SL}dA + \gamma_{LG}\,dA < \gamma_{SG}\,dA \qquad [1.13]$$

where,

γ_{SL}, is the surface free energy associated with the solid-liquid interface, γ_{LG}, is the surface free energy associated with the liquid-gas interface, γ_{SG} is the surface free energy associated with the solid-gas interface, and dA is the incremental area covered by the spreading liquid, respectively.

Upon dividing Equation [1.13] by dA, Equation [1.14] is determined.

$$\gamma_{SL} + \gamma_{LG} < \gamma_{SG} \qquad [1.14]$$

From Equation [1.14], the relationship for the spreading coeffiecient, SC, is determined as found in Equation [1.15].

$$SC = \gamma_{SG} - (\gamma_{SL} + \gamma_{LG}) \qquad [1.15]$$

If Equation [1.15] is positive, the process is spontaneous and therefore the liquid will wet the surface. The method of contact angle measurement can be accomplished by using a goniometer. Once the contact angle of a liquid with a known surface energy is measured, the surface free energy of the corresponding surface can be easily obtained using Young's equation.

A typical example of a liquid wetting a surface can be thought of in the following manner. Immediately after waxing an automobile, any water coming in contact with the car's surface "beads up". In other words, the waxed surface impedes wetting and inhibits spreading. The lower the water contact angle, the higher the surface free energy of the surface, and the greater the extent of wetting for a given substrate and liquid combination. The liquid tends to spread over the high surface free energy substrate in an effort to minimize the total free energy associated with the solid—liquid system.

Through the analysis of contact angles and surface free energies, a useful parameter termed the thermodynamic work of adhesion can be obtained. The thermodynamic work of adhesion is the measure of the energy per unit area required to separate an adhesive—substrate pair from one another resulting in the creation of two

new surfaces . Figure 5, shows the creation of two new surfaces from an original surface.

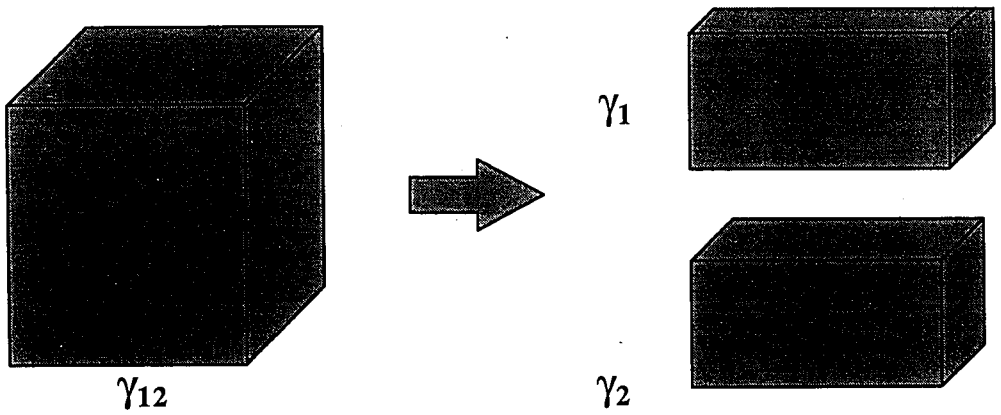

Figure 5. Diagram depicting the separation of a substrate, γ_1, from an adhesive, γ_2 at an interface, γ_{12} into two new surfaces according to the thermodynamic work of adhesion argument. The surface free energy of each surface is expressed as a γ term.

The thermodynamic work of adhesion can be related to the surface free energies of the elastic bodies through the Dupree[15] equation found below :

$$-\Delta G_{12} = W^{12} = \gamma_1 + \gamma_2 - \gamma_{12} \qquad [1.16]$$

where,

γ_1 and γ_2 are the surface free energies of the substrate and adhesive, respectively, whereas, γ_{12} is the surface free energy associated with the interface.

Recently, two different techniques have been used in order to calculate the contact angles between a liquid and a solid pair. The results yield an understanding of the intermolecular interactions that exist at the surface. The first technique is the Two Liquid Probe Method and the second method is the Three Liquid Probe Method. The advantage of the Three Liquid Probe Method over the Two Liquid Probe Method was demonstrated by Good[16]. Good's Three Liquid Probe Method allows for the calculation of the individual acid and base components of the surface free energy in addition to the dispersive component. In this method, three liquids are utilized, one apolar and two polar in nature.

Lloyd[17] has presented a review of experimental techniques in order to characterize both the acid-base and Lifshitz-Van der Waals or dispersive forces acting at an interface. Acid-base interactions occur between electron acceptors, acidic sites, and electron donors, basic sites as well as hydrogen bonding. On the other hand, the Lifshitz

Van der Waals interactions take account for any electromagnetic interactions due to oscillating, permanent, or induced dipoles. Therefore, the total thermodynamic work of adhesion given in Equation [1.16] above, can also be viewed as the addition of the individual force contributions due to the acid-base and Lifshitz-Van der Waals components, respectively.

Much debate currently exists over the exact mechanisms and origins of adhesion and adhesive strength. Kinloch[18] has provided a substantial review on the four types of mechanisms believed to be responsible for the adhesive strength. The four frequently debated interfacial adhesion mechanisms are the mechanical interlocking, diffusion, electronic, and adsorption theories.

To fully understand the adhesive strength both the surface free energy of the interface as well as the fracture energy need to be examined. The surface free energy γ, is typically measured in mJ/m^2, whereas the interfacial fracture energy $G_{I/IIC}$ is found to be in units of J/m^2. The three orders of magnitude difference between γ and $G_{I/IIC}$ can be attributed to the sub-surface damage that occurs. Evans et al.[19] have developed preliminary models looking into other effects such as roughness, segregation, and plasticity. Currently, no comprehensive model exists to fully explain the relationship between the thermodynamic work of adhesion and interfacial fracture energy. Maugis[20] has done extensive research on sub-critical crack growth and on the relation between the fracture energy and surface energy. For interfaces, Maugis developed the relation found in Equation [1.17] below:

$$G = W^a [1 + \phi(v)] \quad [1.17]$$

where,

G is the fracture energy, W^a is the thermodynamic adhesion, ϕ is a parameter related to the viscoelastic losses at the crack tip, and v is the crack growth velocity.

Therefore, the prediction from this theory would suggest a linear dependence between the fracture energy and the thermodynamic work of adhesion. However, this linear dependence is not always observed[11]. Schultz[21] has shown that the orientation of the polymer chains at the interface can change the surface free energy and hence alter the adhesive strength. A shortcoming with the theory developed by Maugis is that surface roughness is not considered. Maugis' theory would work well for elastomeric materials on glass.

Azimi et al.[22] and Phattanarudee[23] have utilized the Three Liquid Probe Method in order to characterize the intermolecular interactions existing between many die-attach adhesives on various surfaces. The thermodynamic work of adhesion was then correlated with the interfacial fracture energy and a reasonable correlation was found to exist. This technique can be applied to examine the interfaces of composites, adhesives, and surface coatings.

Moisture can significantly affect the adhesion values that are determined. An adhesive could be either hydrophobic or hydrophilic in nature. Therefore, the adhesive

strength of the adhesive in the presence of moisture, can increase if the adhesive is hydrophilic or decrease if it's hydrophobic. Kinloch[24] has measured the thermodynamic work of adhesion for various surfaces in the presence of liquids. Each interface may exhibit different values of the thermodynamic work of adhesion depending on the liquid used as well as on the distribution of intermolecular forces associated with the interface being examined. Kinloch's relation for interfacial stability is shown in Equation [1.18]:

$$W_{AL} = \gamma_{aL} + \gamma_{sL} - \gamma_{as} \qquad [1.18]$$

where,

W_{AL} is the thermodynamic work of adhesion in the presence of a liquid, γ_{aL} is the interfacial surface free energy between the adhesive and liquid, γ_{sL} is the interfacial surface free energy between the substrate and liquid, and γ_{as} is the interfacial surface free energy between the adhesive and substrate.

Such a relationship captures the competition between polymer and moisture adsorbing on a surface.

1.5 Microelectronics Packaging

The field of microelectronics packaging has been shifting its resources away from conventional ceramic packages and towards plastic packaging. Today, more than 97% of all integrated circuits are protected by plastic packages. Plastic packages offer many advantages over ceramic packages. Specifically, plastic packages offer an overall lighter package weight and are extremely economical to manufacture. Many interfaces exist within each plastic package. Typical interfaces of interest are shown in Figure 6. At each interface, the probability of failure is greatly increased due to mismatches in elastic moduli and coefficients of thermal expansion. Upon exposure to elevated temperatures, the propensity or probability for failure is significantly increased.

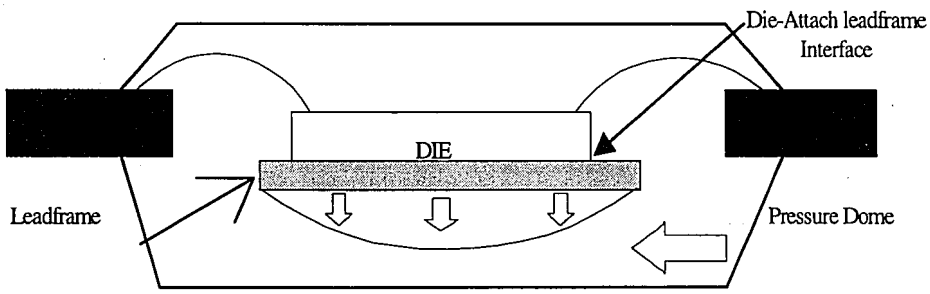

Figure 6. Typical Microelectronics Plastic Package showing the interface of interest and vapor pressure during solder reflow.

The methods of package fabrication and processing are extremely important[25]. Contamination of any of the components in the package can result in failure of the entire device[26]. Resulting failures can be either electrical or mechanical in origin. Electrical failure in plastic packages often occurs due to corrosion of the metallization, which can result in malfunctioning of the wire bonds, whereas, mechanical failure is attributed to the actual cracking of the plastic package.

During plastic package fabrication, the silicon die is attached to the leadframe material through the use of the die-attach adhesive. Leadframe materials are typically high-purity Cu alloys, which are used in order to provide a high degree of electrical and thermal conductivity throughout the microelectronic plastic package. Die-attach adhesive formulations usually consist of silver (Ag) particles dispersed within an epoxy resin. Typically, the weight percentage of silver (Ag) used in these die-attach formulations is greater than 70 percent. Through the wire bonding process, the electrical connection is made between the leadframe and the silicon die.

Therefore, the die-attach adhesive—leadframe interface is one of the most critical interfaces contained within the plastic package. The wires are joined to the leadframe substrate through the wire bonding process.

During the solder or vapor phase reflow processes, moisture which has diffused into the package becomes vaporized due to the elevated temperature exposure (Figure 6). Typically, temperatures may reach between 200 and 215°C during these reflow processes. The vaporized pocket of moisture, between the die and die-pad, continues to expand until it finally ruptures. Upon rupture, a loud audible "popping" sound can be

heard and delamination occurs. This common occurrence in the microelectronic packaging industry is called the "popcorn effect". The popcorn effect has been extensively reviewed in the literature for various package geometries[27,28,29].

Specifically, as shown in Figure 6, the interface between the die-attach adhesive and leadframe needs to be reliable. This interface should be able to withstand the required processing and in-service conditions for each package geometry.

1.6 Objectives

The objectives of this research are threefold:

1) To examine the effect of high temperature and humidity exposure on room temperature adhesion in filled-epoxy die-attach adhesives.

2) To determine whether the thermodynamic work of adhesion can predict the drop in adhesion due to moisture.

3) To determine if a correlation exists between the thermodynamic work of adhesion, W^a, and the interfacial fracture toughness, $G_{I/IIC}$ when using the same adhesive and cleaning the surface.

2. EXPERIMENTAL PROCEDURE

2.1 Materials

The three silver-filled die-attach adhesives examined in this study were Ablebond AB84-1LMISR4 from Ablestik, Epo-Tek H35-175MP from Epoxy Technology, and KO111 from Dexter Electronics. The Ag filler contents for AB 84-1, H35, and KO111 are 70-85, 73, and 70-80 weight percent, respectively. The cure schedules for the three die-attach adhesives are found in Table II.

The FR-4 resin was obtained from IBM and was 1080 cloth-style, which consists of glass fiber mat and pre-preg epoxy resin. The FR-4 laminates (50 layers) were cured according to Table I. Final laminate thickness was nominally 3.00 mm. The IBM Cu foil (one ounce thick) when utilized, was laminated to the 50 layers of FR-4.

Leadframe materials utilized in this study were Olin C-194 Cu Extra Spring Relief Annealed with a thickness of .152 mm from Olin Corporation and a Ni/Pd coated Olin C-194 Cu alloy with a thickness of .127 mm from Texas Instruments. The Ni thickness was approximately 1143 μm and the Pd thickness was 76.2 μm.

2.2 Three Liquid Probe Method

The Three Liquid Probe Method was used in order to characterize the surfaces used in this work. Phattanarudee et al.[23] have determined the contact angles for the surfaces used in this research. For the surface characterization, three liquids; two polar

and one apolar were used. The polar liquids were water and ethylene glycol, whereas the apolar liquid was diiodomethane. This enables the calculation of the thermodynamic work of adhesion, W^a for each adhesive—substrate pair. Contact angles were measured using an automated video contact angle goniometer developed by Connelly Applied Research. This instrument introduces and withdraws the liquid with a computer-controlled syringe pump, and stores the image of the drop. The advancing or receding contact angle can be determined by using a proprietary sub-pixel interpolation method. A sessile drop was advanced six times by pumping the liquid at 1μL/sec. The contact angle was measured for both sides of the drop. For each surface, the advancing angles were averaged from drops placed on three different locations of the surface.

2.3 MMB Test Method

Three different silver-filled die-attach adhesives were used: AB84-1LMISR4 from Ablestik, Epo-Tek H35-175MP from Epoxy Technology, and KO111 from Dexter Electronics. The adhesives were tested on IBM Cu foil, which was attached to 50 layers of FR-4 composite (glass fiber mat & epoxy resin). The FR-4 laminates were cured in a Tetrahedron Thermal Press under both heat and pressure according to the cure schedule found in Table I. The specimen geometry was that of a MMB sandwich. A pre-crack was started on one surface by application of Teflon mold release spray and a die-attach adhesive was deposited on the remaining area of that same surface. The adhesive was then degassed in a vacuum oven under temperature.

The leadframe surfaces used were a Ni/Pd coated Cu, C194, leadframe material from TI with a thickness of .127 mm and a C194 Extra Spring Relief Annealed Cu alloy from Olin with a thickness of .152 mm. The interfacial fracture toughness was measured using the Mixed-Mode Bending Fixture developed by Reeder and Crews[8]. The fixture was attached to a Screw-Driven Instron Machine. The interfacial fracture energy was then determined. Both dry and wet MMB samples were tested. For the wet sample conditioning, the samples were placed in an Environmental Chamber from Ecosphere for 168 hours @ 85°C/85%RH.

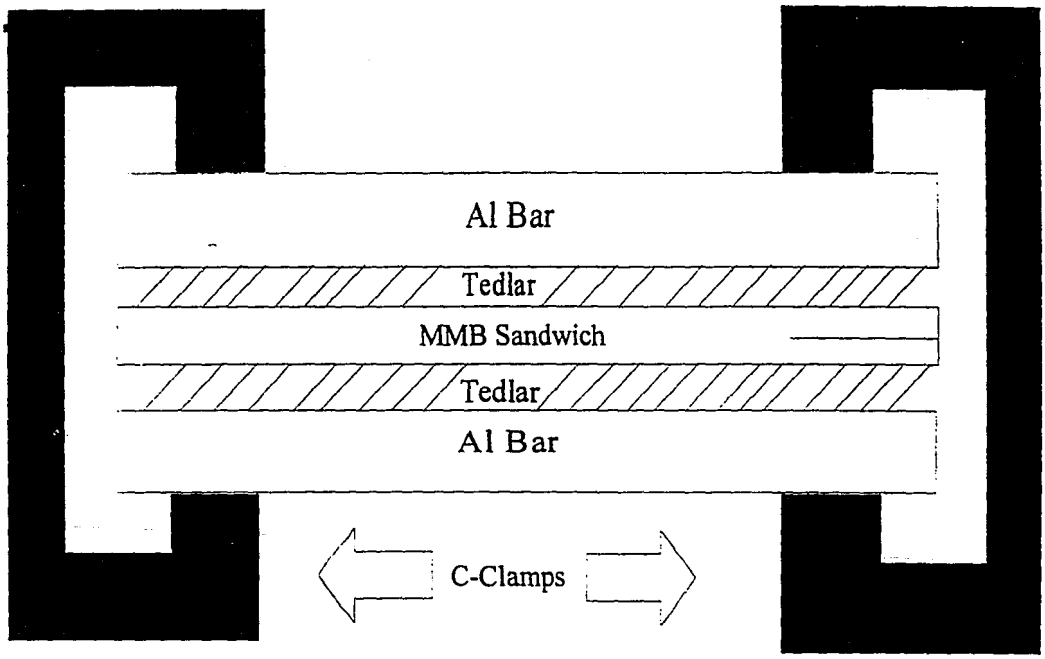

Figure 7. Mixed-Mode Bending Specimen Preparation.

Step	Temp	Temp Rate	Force	Force Rate	Tool Temp	Time
1	350F	500	30.0	600	OFF	1 Hr.
2	70F	6	30.0	600	OFF	5 min.
3	OFF	200	OFF	600	OFF	OFF

Table I. Cure Schedule for FR-4 Laminates.

Die-Attach Adhesives	Recommended Cure	Cure Schedule Used
AB84-1LMISR4	1 Hour @ 175°C	1 Hour @ 175°C
EPO-TEK H35-175MP	1 Hour @ 180°C	1 Hour @ 180°C
HYSOL KO111	3 minutes @ 150°C	½ Hour @ 150°C

Table II. Cure Schedules Utilized in this Study.

2.3.1 Preparation of MMB IBM Cu

AB 84-1LMISR4 from Ablestik, Epo-Tek H35, and K011 from Dexter were cured on IBM Cu foil. In order to supply some stiffness, the Cu foil was laminated to 50 layers of 1080 cloth-style FR-4, which consists of glass fiber mat and pre-preg epoxy resin. The laminates were cured under heat and pressure, in a thermal press from Tetrahedron, according to the curing schedules found in Table I.

The laminates were then machined into 152.4 mm long by 25.4 wide and 3.00 mm thick rectangular pieces. The test samples utilized were in a sandwich geometry. On one half of the MMB sandwich, Teflon mold release spray was applied to an area of 50.8 mm and the corresponding die-attach adhesive was then dispensed on the rest of the area. The Teflon release served as the pre-crack region. The bond-line adhesive thickness was .254 mm.

This half was then placed in a vacuum oven and degassed under a pressure of 29mm Hg and a temperature of 80°C. After degassing, the adhesive was smoothed over the surface using a tongue depressor. To control the bond line thickness, .254 mm spacers were used. The second half of the MMB sandwich was then pressed together with the first half. Next, the sandwich was clamped with C-clamps between Tedlar release paper and two Al bars (177.8 mm long, 24.9mm wide, and 18.38mm thick) in order to prevent warpage and to maintain alignment during the curing process. The entire structure was then placed into a convection oven and cured according to the cure schedules found in Table II.

After curing the samples were allowed to cool down to room temperature. On both sides of the sandwich, a brittle correction fluid, White Out™, was applied so that crack growth could be monitored.

For each adhesive on IBM Cu, the interfacial fracture energy was measured under both dry and wet (168 hrs @ 85°C/85% RH) conditions. For the wet conditioning, an Environmental Chamber from Ecosphere was used. Both types of MMB testing were performed at room temperature.

2.3.2 MMB Leadframe Preparation

The leadframe materials used in this study were Olin C-194 Cu alloy (.152 mm thickness) and Olin C-194 Cu alloy coated with Ni and Pd (.127 mm thickness).

The MMB leadframe sandwiches were cured in a convection oven like the IBM Cu foil was in Section 2.1.1. After curing, however, the leadframe sandwich was attached (at room temperature) to the to the FR-4 arms with a cyanoacrylate ester. For each adhesive and surface, the interfacial fracture energy was measured under both dry and wet (168 hrs @ 85°C/85% RH) conditions. Both types of MMB testing were performed at room temperature.

2.3.3 Leadframe Surface Preparation

In order to examine how the cleanliness of the leadframe surface affects the adhesive strength, each leadframe substrate was cleaned using a U-V ozone cleaning oven, after being cleaned in hot isopropanol at 80°C to remove any grease or oils. The two leadframe surfaces used were Olin C-194 Cu alloy (.152 mm thickness) and Olin C-194 Cu alloy coated with Ni and Pd (.127 mm thickness), with the corresponding die-attach adhesives being AB84-1, Epo-Tek H35, and Hysol KO111. For the U-V ozone cleaning, times of 0, 5, and 10 minutes were utilized. The only difference between the two leadframe substrates used was that the Ni/Pd coated leadframe surface from TI possessed an anti-tarnishing agent which was removed by using a 5 M rinse in HCl, followed by a rinse in Chromatography Grade Methanol, and finally two DI water rinses.

2.4 Loading Procedure

The MMB sandwich specimens were then tested with the Mixed Mode Bending (MMB) Testing Fixture, which was developed by Reeder and Crews[8] on a Screw-Driven Instron Machine. The Instron applied the loads to the specimens at a cross-head speed of 2.00 mm per minute. The sample was loaded until a slight decrease in load was detected and then quickly unloaded. The crack length and deflection at the loading point were noted and the sample was then reloaded. Typically, five measurements were obtained in this fashion for each MMB specimen. The data obtained was then plugged into Equations [2.1] and [2.2], and the interfacial fracture toughness, $G_{I/IIC}$ was determined for each die-attach adhesive.

$$G_{IC} = \frac{3P^2 (a + \chi_I h)^2}{B^2 E_{11} h^3} \left[(1 - \frac{c + b}{L})F_2 - \frac{c}{b} F_1\right]^2 \quad [2.1]$$

$$G_{IIC} = \frac{9P^2 (a + \chi_{II} h)^2}{4B^2 E_{11} h^3} \left[(1 - \frac{c + b}{L})F_2 + \frac{c}{b} F_1\right]^2 \quad [2.2]$$

where,

b, c, and L are fixture parameters (m), see Figure 3.

a, is the initial crack length from the center loading point of the center hinge position to the corresponding crack tip (m).

χ_I and χ_{II}, are correction factors for Mode I and Mode II, respectively.

h, is the half-thickness of the specimen (m).

F_1 and F_2, are correction factors due to the large deflection of the loading arms.

Figure 8 below, is a typical load versus displacement plot which is obtained during a typical mixed-mode bending test.

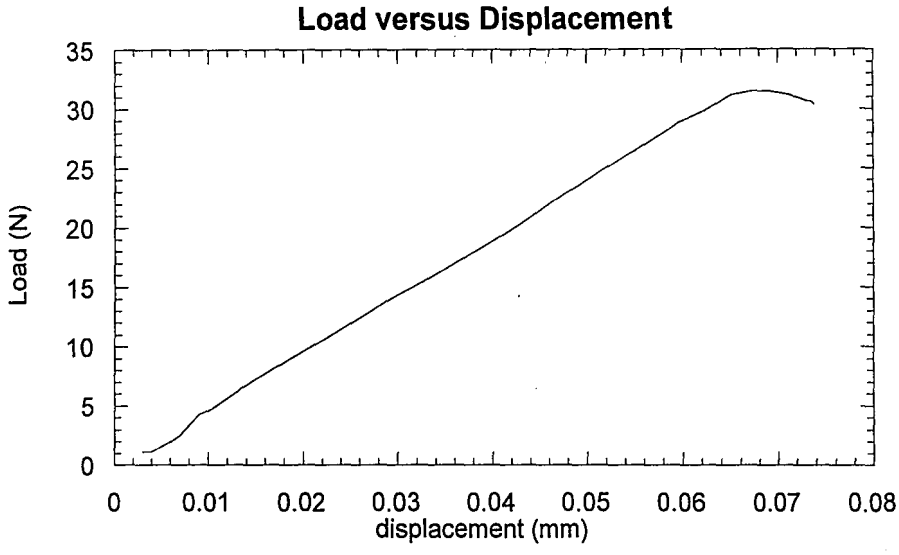

Figure 8. Typical load versus displacement plot generated from MMB test.

2.5 Weight Gain Sample Preparation and Testing

Weight gain experiments were conducted for AB 84-1LMISR4, Epo-Tek H35, and KO111. Samples were machined with the dimensions being 20.0 mm long, 6.00 mm wide and 4.00 mm thick. For the three die-attach adhesives, five samples of each one were placed in an Ecosphere Environmental Chamber and exposed to moisture and temperature conditioning of 85°C/85%RH. Prior to placing the samples in the environmental chamber, the dry weight was recorded for each one. The samples were then placed into the chamber at 85°C/85%RH and removed intermittently to be weighed with a scale from Denver Instruments Company. The duration of each test was approximately 500 hours. The percent weight gain versus time was then determined for each die-attach adhesive.

2.6 DMA Sample Preparation and Testing

Dynamic Mechanical Analysis (DMA) samples for each of the three die-attach adhesives used in this study were cured in a silicone mold and were tested dry and also after a conditioning of 85°C/85%RH for 168 hours. Each sample was tested from -100 to 250°C, on the RDA II from Rheometrics using a heating rate of 10°C/minute and a strain rate of 0.1%. For DMA testing, the stress and strain relationship are governed by Equations [2.3] and [2.4] below:

$$\sigma(t)= \varepsilon_o G_1 \sin(\omega t) + \varepsilon_o G_2 \cos(\omega t) \qquad [2.3]$$

$$\text{and} \quad G_1 = \frac{\sigma_o}{\varepsilon_o} \cos\delta \text{ and } G_2 = \frac{\sigma_o}{\varepsilon_o} \sin\delta \qquad [2.4]$$

where,

σ is the stress, ε is the strain, ω is the frequency, and t is the time. Also, G_1 is defined as the storage modulus which is in phase with the strain and G_2 is the loss modulus which is 90° out of phase with the strain.

The complex modulus, G*, is determined through the addition of the G_1 and G_2 components. The complex modulus is found in Equation [2.5].

$$G^* = G_1 + iG_2 \qquad [2.5]$$

where,

G* is the complex modulus, G_1 is the storage modulus, G_2 is the loss modulus, and where i is the square root of -1.

Equation [2.6] shows the method by which the tan δ peak is generated during DMA testing. Tan δ is simply the ratio of the loss to storage moduli, respectively.

$$\tan \delta = \frac{G_2}{G_1} \qquad [2.6]$$

3. RESULTS AND DISCUSSION

3.1 Surface Characterization

Phattanarudee[30] has characterized the dispersive and polar components of the surface free energy for various leadframe substrates by utilizing the three liquid probe method. The three liquids used were diiodomethane, ethylene glycol, and water, respectively. The surface free energies for two leadframe substrates are found in Table III, below.

Substrate	γ_s^{LW} (mJ/m^2)	γ_s^+ (mJ/m^2)	γ_s^- (mJ/m^2)
Ni/Pd finish on Cu	28.7	0.1	2.0
Olin C-194 Ex-Spring Hard	21.8	0.4	0.0

Table III. Dispersive and polar components of the surface energy for leadframe substrates.

Figures 9 and 10, show the interfacial fracture energy, $G_{I/IIC}^{inter}$ versus the thermodynamic work of adhesion, W^a, for various silver-filled epoxy die-attach adhesives from Early et al[31]. This work suggests that a simple relation between the thermodynamic work of adhesion and interfacial fracture energy does not exist as suggested by Maugis[20].

Work of Adhesion Correlation for FR-4

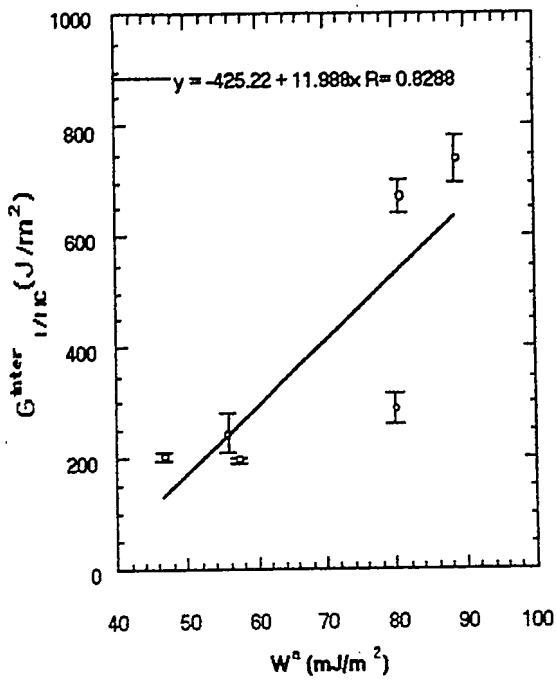

Work of Adhesion Correlation For IBM Cu

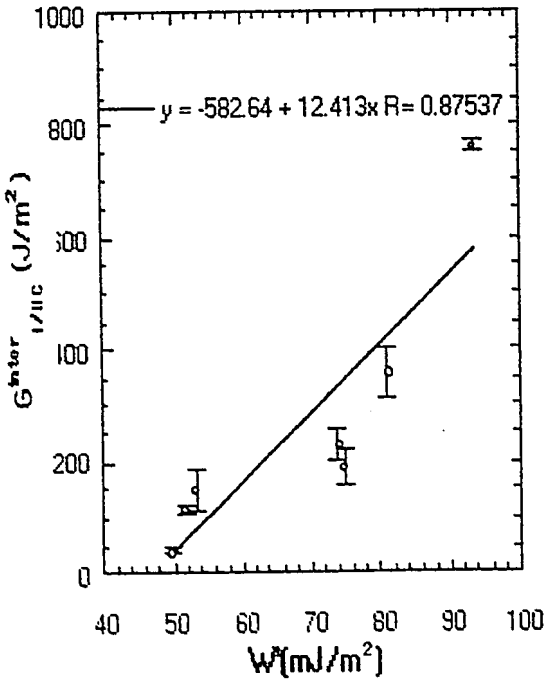

3.2 MMB IBM Cu (Dry/Wet)

Table IV, shows the critical interfacial fracture energy for the silver-filled epoxy die-attach adhesives H35-175MP, AB84-1LMISR4, and KO111 on the IBM Cu foil surface. It was found that the interfacial fracture energy decreased upon exposing the mixed mode bending samples to a temperature and moisture condition of 85°C and 85% RH for 168 hrs. This is consistent with the lower glass transition values that were observed after conditioning these adhesives for 85°C/85%RH during the dynamic mechanical analysis found in Section 3.5. After the moisture enters into the die-attach adhesive, it plasticizes the matrix and causes the Tg reduction, which in effect causes the decrease in $G_{I/IIC}^{inter}$, seen in Table IV. In Section 3.1, the values of the dispersive and polar components of the surface free energy are in units of mJ/m^2, whereas, the units of $G_{I/IIC}^{inter}$, in Table IV are in J/m^2. This order of magnitude difference between γ and $G_{I/IIC}^{inter}$ can be attributed to the energy that is dissipated due to sub-surface damage mechanisms.

Adhesive	$G_{I/IIC}^{inter}$ (J/m^2) Dry as molded on IBM Cu foil	$G_{I/IIC}^{inter}$ (J/m^2) Conditioned 85°C/85%RH for 168 hrs On IBM Cu foil
H35-175MP	447 ± 57	303 ± 50
AB84-1LMISR4	358 ± 25	231 ± 35
KO111	230 ± 32	202 ± 37

Table IV. $G_{I/IIC}^{inter}$ (J/m^2) for ambient versus conditioned, 85°C/85%RH for 168 hrs, on IBM Cu surface.

3.3 MMB Leadframe (Dry/Wet)

MMB samples of H35-175MP, AB84-1LMISR4, and KO111 were made consisting of FR-4 arms and a testing surface consisting of Olin C-194 Cu alloy (.152mm thick). The effect of U-V ozone surface cleaning for the Olin C-194 Cu alloy (.152mm thick) was found to be negligible. U-V ozone cleaning times of 0, 5, and 10 minutes were utilized. The leadframe materials were supported by FR-4 arms during the Mixed-Mode Bending tests due to the extreme ductility of the thin Cu substrates. The observed fracture surfaces were adhesive in nature.

The results found in Tables V and VI, show that cleaning the Cu substrate with U-V ozone prior to bonding, does not influence the interfacial fracture energy significantly. Cleaning the substrates with U-V ozone, should lower the contact angles and hence increase the $G_{I/IIC}^{inter}$, however improved adhesion was not generally observed. Any contamination, which exists on the Cu leadframe surface prior to bonding, may be absorbed within the epoxy die-attach adhesive. Thus, making all the surfaces behave identically during the Mixed-Mode Bending tests.

Adhesive	$G_{I/IIC}^{inter}$ (J/m^2) UV= 0 minutes	$G_{I/IIC}^{inter}$ (J/m^2) UV= 5 minutes	$G_{I/IIC}^{inter}$ (J/m^2) UV= 10 minutes
H35-175MP	401 ± 40	351 ± 33	380 ± 32
AB84-1LMISR4	357 ± 44	308 ± 31	358 ± 45
KO111	271 ± 54	263 ± 30	316 ± 28

Table V. Effect of U-V ozone cleaning time on ambient $G_{I/IIC}^{inter}$ for H35-175MP, AB84-1LMISR4, and KO111 under ambient conditions on Olin C-194 Cu surface.

Adhesive	$G_{I/IIC}^{inter}$ (J/m^2) UV= 0 minutes	$G_{I/IIC}^{inter}$ (J/m^2) UV= 5 minutes	$G_{I/IIC}^{inter}$ (J/m^2) UV=10 minutes
H35-175MP	327 ± 23	370 ± 32	328 ± 25
AB84-1LMISR4	319 ± 22	310 ± 37	297 ± 37
KO111	172 ± 28	226 ± 43	211 ± 33

Table VI. Effect of U-V ozone cleaning time on $G_{I/IIC}^{inter}$ for H35-175MP, AB84-1LMISR4, and KO111 after conditioning of 85°C/85%RH for 168 hrs on Olin C-194 Cu surface.

Finally, Mixed-Mode Bending samples of H35-175MP, AB84-1LMISR4, and KO111 were processed consisting of FR-4 arms and Olin C-194 Cu alloy coated with Ni and Pd from TI (.127mm thick). It was found that exposing these samples to a condition of 85°C/85%RH for 168 hrs as opposed to ambient, significantly lowered the critical interfacial fracture energy, $G_{I/IIC}^{inter}$ as seen in Table VII. Once again, the failures were adhesive in nature. In Section 3.4, it was seen that H35-175MP, AB84-1LMISR4, and KO111 all absorb water when exposed to 85°C/85%RH for 168 hrs and in Section 3.5 the glass transition temperatures, Tg's, were found to decrease as well. Once again, the moisture from the conditioning step of 85°C/85%RH became absorbed within the epoxy matrix and plasticizes it; thereby lowering the interfacial fracture energy during the mixed-mode bending test.

Adhesive	Dry as molded $G_{I/IIC}^{inter}$ (J/m^2)	Conditioned at 85°C/85%RH for168hrs $G_{I/IIC}^{inter}$ (J/m^2)
H35-175MP	357 ± 32	243 ± 25
AB84-1LMISR4	252 ± 29	175 ± 24
KO111	137 ± 25	113 ± 22

Table VII. $G_{I/IIC}^{inter}$ on Olin C-194 Ni/Pd from TI for H35-175MP, AB84-1LMISR4, and KO111 under both dry and wet conditions.

Adhesive	$G_{I/IIC}^{inter}$ (J/m^2) IBM Cu Foil	$G_{I/IIC}^{inter}$ (J/m^2) Cu Alloy	$G_{I/IIC}^{inter}$ (J/m^2) Ni/Pd on Cu Alloy
H35-175MP	447 ± 57	401 ± 40	357 ± 32
AB84-1LMISR4	358 ± 25	357 ± 44	252 ± 59
KO111	230 ± 32	271 ± 54	137 ± 25

Table VIII. Summary table of $G_{I/IIC}^{inter}$ (J/m^2) under ambient conditions for H35-175MP, AB84-1LMISR4, and KO111 on various surfaces.

Adhesive	$G_{I/IIC}^{inter}$ (J/m^2) IBM Cu Foil	$G_{I/IIC}^{inter}$ (J/m^2) Cu Alloy	$G_{I/IIC}^{inter}$ (J/m^2) Ni/Pd on Cu Alloy
H35-175MP	303 ± 50	327 ± 23	243 ± 25
AB84-1LMISR4	231 ± 35	319 ± 22	175 ± 24
KO111	202 ± 37	172 ± 28	113 ± 22

Table IX. Summary table of $G_{I/IIC}^{inter}$ (J/m^2) after conditioning of 85°C/85% RH for 168 hours for H35-175MP, AB84-1LMISR4, and KO111 on various surfaces.

3.4 Weight Gain Experiments

Figure 11, shows a plot of the percent weight gain versus time under an 85°C/85% RH condition for AB84-1LMISR4, H35-175MP, and KO111, respectively. Both AB84-1LMISR4 and H35-175MP exhibit a 1.3% weight gain after 500 hours, whereas KO111 shows a quick increase to .5 weight percent followed by a decrease to -.2 weight percent after approximately 500 hours. A 1.3 weight percent increase is significant in these Ag-filled epoxy die-attach adhesive systems, since the matrix is composed of primarily silver. In these systems, Ag comprises anywhere from 70 to 80 weight percent, and therefore the epoxy matrix and interphase are the only two sources for moisture absorption in these systems. In addition, absorbed water may react with the epoxy and open unreacted oxirane rings[32].

Significant research has been conducted into examining the moisture absorption of epoxy resins. El-Sa'ad et al.[33] have examined the moisture absorption characteristics of rubber particulate filled epoxy adhesives. The authors found that the maximum moisture content varied significantly with increased temperature and relative humidity. Barton and Pritchard[34] have also studied the moisture characteristics of epoxy resins. They found that for Epikote828/MPD, the rate of absorption and the equilibrium moisture level increased with increasing relative humidity at a temperature of 50°C. Therefore, absorbed moisture levels can be detrimental to the mechanical properties of the epoxy system.

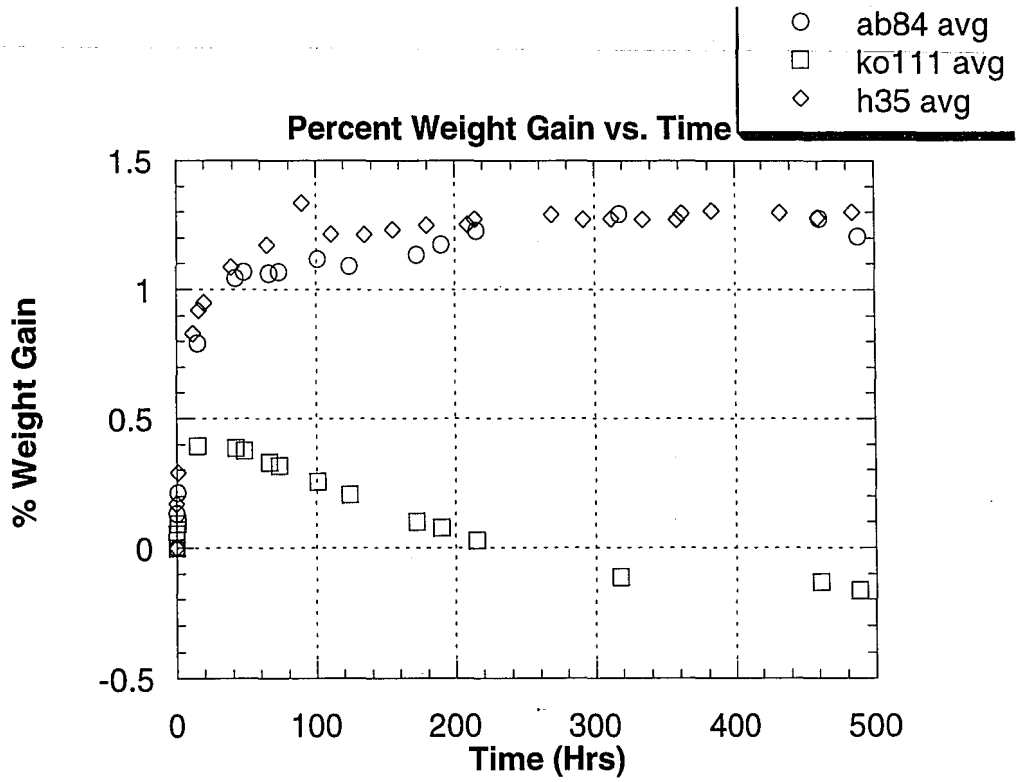

Figure 11. Percent weight gain versus time at 85°C/85% RH for H35-175MP, Ablebond 84-1LMISR4, and Dexter Hysol KO111.

3.5 DMA Testing

The dynamic mechanical analysis plots for AB84-1LMISR4, H35-175MP, and KO111 are found in Figures 12 to 14, respectively. Each plot contains a comparison of dry versus wet data. The upper portion of each figure contains the G' or storage modulus while the lower portion contains the tan delta curves which is a measure of the ratio of the loss and storage moduli. For all three silver die-attach adhesives, it was found that a decrease in the Tg occurred upon exposing the materials to the wet condition of 85°C/85%RH for 168 hrs when compared to the dry or ambient condition. The Tg reduction for AB-84 was from 60 to 50°C, 130 to 120°C for H35, and finally 70 to 65°C for KO111. This reduction in the Tg can be attributed to the absorption of water into the epoxy matrix and into the interphase region which occurs during the exposure to the increased temperature and humidity levels. Water may migrate from the matrix and collect at the interphase region, between the epoxy matrix and Ag particles. The water enters into the epoxy and acts as a plasticizer, thereby lowering the Tg, and hence the mechanical properties.

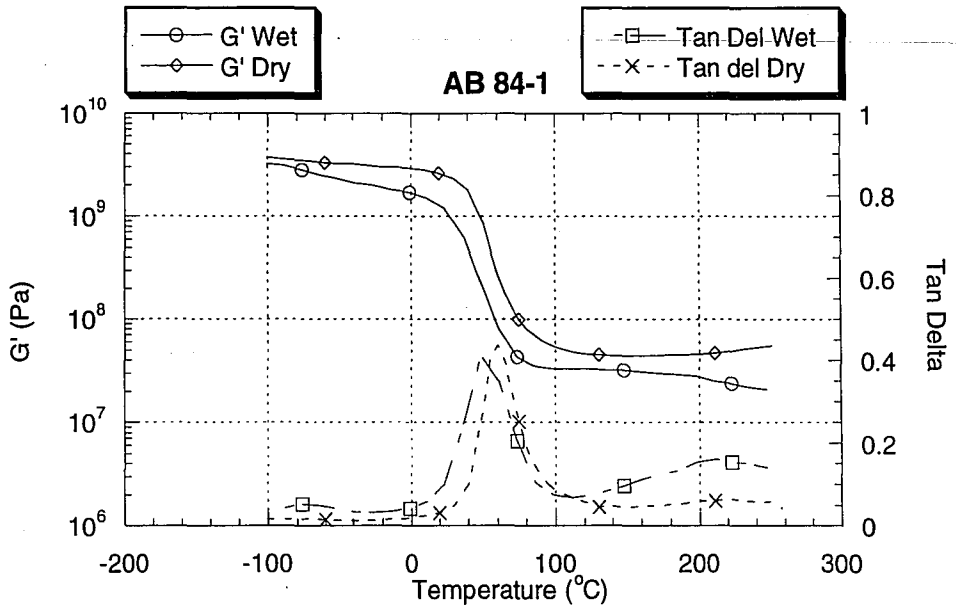

Figure 12. Dry versus Wet RDA plot of AB 84 showing G' and tan delta. The RDA reveals a 10°C reduction in the glass transition temperature when exposed to 85°C/85% RH for 168 hrs.

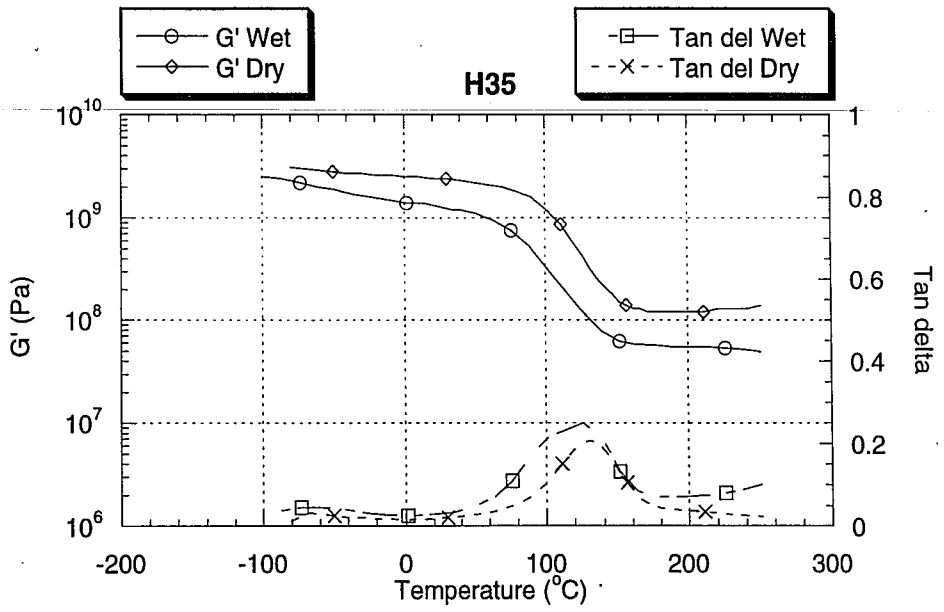

Figure 13. Dry versus Wet RDA plot of H35 showing G' and tan delta. RDA reveals a 10°C reduction in the glass transition temperature when exposed to 85°C/85% RH for 168 hrs.

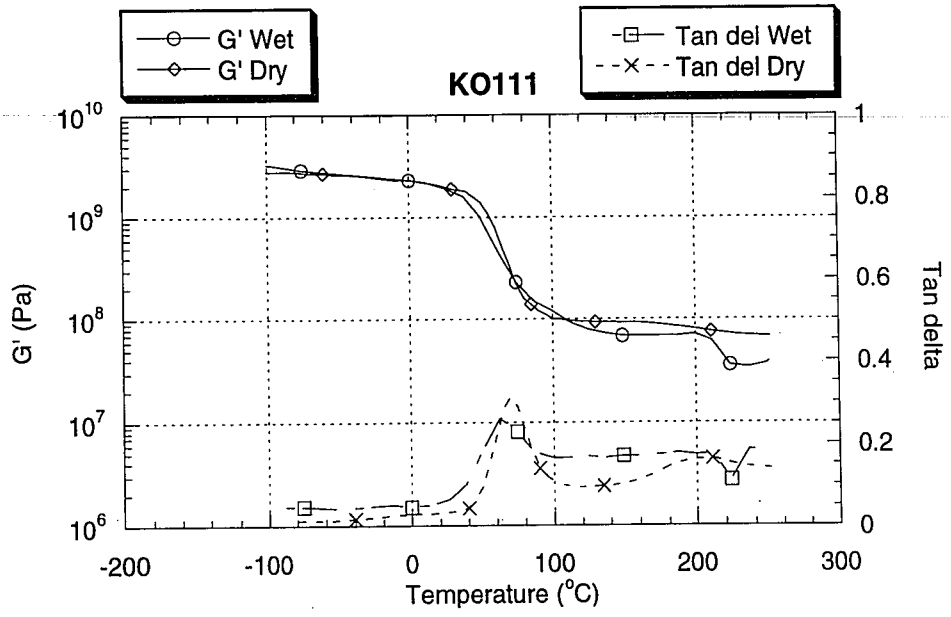

Figure 14. Dry versus Wet RDA plot of KO111 showing G' and tan delta. RDA reveals a 5°C reduction in the glass transition temperature when exposed to 85°C/85% RH for 168 hrs.

4. CONCLUSIONS

1) It was found that the interfacial fracture energy, $G_{I/IIC}^{inter}$, decreased upon exposing MMB samples to an increased temperature and humidity condition due to the plastization of the epoxy matrix by absorbed moisture.

2) Cleaning Cu leadframe materials with U-V ozone had no significant effect on the adhesive strength in these systems, since the three silver-filled epoxy die-attach adhesives absorbed all surface contamination prior to bonding.

3) The interfacial fracture energy for H35-175MP, AB84-1LMISR4, and KO111, on the Ni/Pd coated Cu surface was found to be lower than on the plain Cu leadframe surface due to the lower surface free energy of the Ni/Pd surfaces.

5. RECOMMENDATIONS FOR FUTURE WORK

To study in detail the fracture micromechanisms that are responsible for energy dissipation in these systems through the use of SEM and to examine the adhesive strength under varying temperature and humidity levels, corresponding to the JEDEC standards.

APPENDIX A

FATIGUE AND INTERFACIAL FRACTURE TOUGHNESS OF ENCAPSULANTS

This Appendix contains data obtained for the SEMATECH Liquid Encapsulant Enhancement (LEE) Project. Specifically, bulk fatigue crack propagation and interfacial fracture toughness results.

INTRODUCTION

Liquid encapsulants and underfill materials are frequently utilized by the microelectronics packaging industry. The current drive for lower costing and higher reliability materials and finished products are driving the industry to encapsulants and underfill materials. Typically, the materials possess a low viscosity, which enables the material to flow into the cavity or joint. Encapsulants and underfills protect the package from the elevated temperature and moisture levels that are experienced during both material processing and service-lifetime. In order to evaluate the mechanical reliability of these materials, both bulk fatigue crack propagation and interfacial fracture toughness testing were accomplished.

EXPERIMENTAL PROCEDURE

Bulk fatigue crack propagation testing was accomplished on Dexter Hysol FP 4450, 4520, and 4511 through the use of a servo-hydraulic Instron materials testing machine containing a five hundred pound load cell and interfaced with software from Fracture Technology Associates in order to monitor crack growth rate and driving force, respectively. The decreasing delta K data for FP 4511, 4520, and 4450 were generated using K^{c}_{max}, whereas, the increasing delta K data were generated using a fixed R at .1 and a K-gradient of + 0.1. The specimen geometry for the fatigue crack propagation testing was of the compact tension (CT) type as can be seen in Figure 15.

The interfacial fracture toughness of FP 4450 and 4511 on various surfaces was examined through the use of the Mixed-Mode Bending Fixture. The specimen geometry was that of a MMB sandwich. The specimen preparation was done in a similar fashion as for the die-attach adhesives (See Section 2). The surfaces examined in this study were FR-4, 8100HD7400 and 8200HD7400 solder masks, and two HP solder fluxes. However, FP 4450 was only examined on the 8100HD7400 solder mask surface. Interfacial fracture toughness testing after both dry, ambient, and wet, 168hrs @ 85°C/85% RH, conditioning was accomplished for FP 4511 on the FR-4, and 8100HD7400 and 8200HD7400 solder masks, respectively. The FP 4511 underfill material on the two HP solder fluxes was only done at the ambient condition. For FP 4450, the only surface studies was the 8100HD7400 solder mask under both dry and wet conditions.

Weight gain experiments were conducted on FP 4450 and FP 4511, respectively. The sample dimensions were 20 mm long by 6.0 mm wide by 4.0 mm thick. Five samples of each material were then placed in the Ecosphere Environmental Chamber from Despatch at 85°C and 85% RH. The samples were removed periodically and weighed with a five digit scale from Denver Instruments Company in order to determine the corresponding weight gain for each sample. The duration of the weight gain testing for both FP 4450 and 4511 lasted for approximately 700 hrs.

Cure schedules employed for the materials in this study were two hours at 150°C for FP 4511, 30 minutes at 125°C, followed by 90 minutes at 165°C for FP 4450, and one hour at 165°C for FP 4520.

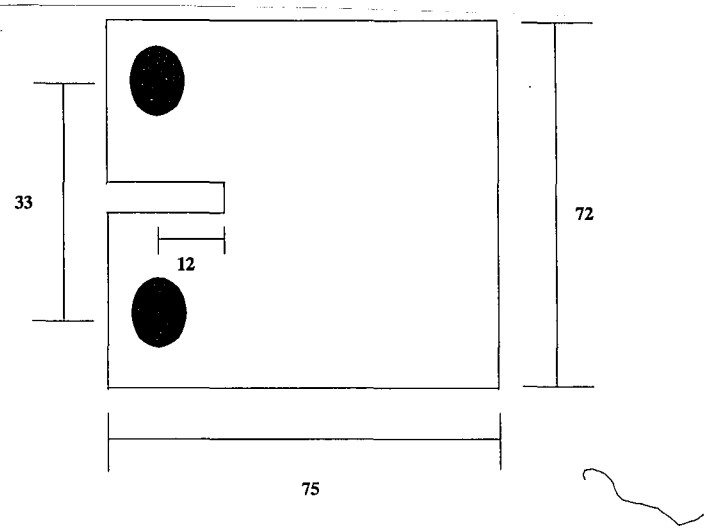

Figure 15. Compact tension specimen geometry used in FCP tests.

Results/Discussion

Figure 16, is a plot of the fatigue crack propagation behavior of FP 4450, 4511, and 4520. From this plot, it is seen that FP 4450 is the most fatigue resistant encapsulant of the three materials tested under cyclic loading conditions.

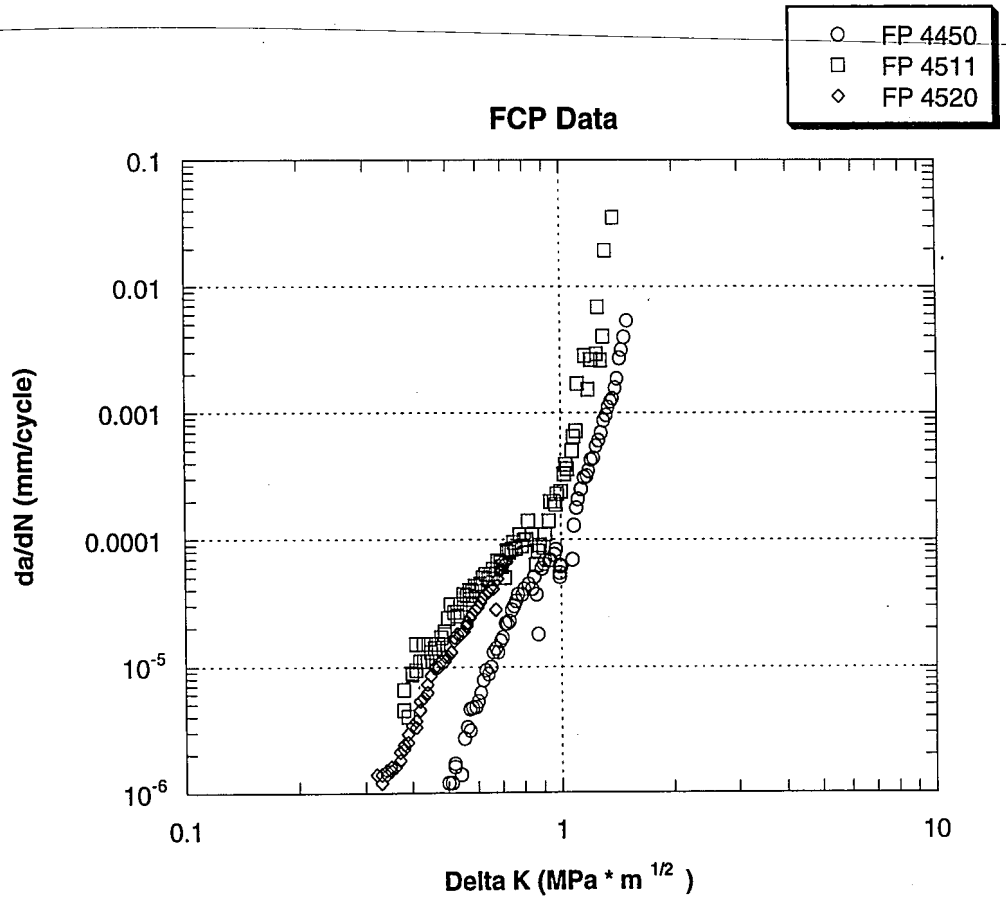

Figure 16. da/dN versus delta k for FP 4450, 4511, and 4520.

Table X, contains interfacial fracture toughness data generated through the Mixed-Mode bending apparatus. It was found that after subjecting the MMB samples to a conditioning of step of 85°C/85%RH for 168 hrs, the adhesive strength significantly decreases when compared to ambient.

Adhesive	$G_{I/IIC}^{inter}$ (Dry)[1] (J/m^2)	$G_{I/IIC}^{inter}$ (Wet)[1] (J/m^2)
4511/FR-4	389 ± 82.6	52.8 ± 20.2
4511/8100HD7400	121 ± 9.5	160 ± 8.5
4450/8100HD7400	130 ± 36.8	74.0 ± 15.4
4511/8200HD7400	97.4 ± 31.0	81.5 ± 28.2
4511/FR-4/X[2]	142 ± 51.6	N/A
4511/FR-4/Y[2]	79.2 ± 23.4	N/A

Note: 1. Dry condition was ambient, whereas wet condition was after 168 hrs @ 85°C/85%RH.

Note: 2. X and Y are both HP solder fluxes with X flux (pure) applied directly to surface with doctor blade and Y dipped into 5 wt% isopropanol flux solution with both sides exposed.

Table X. Table showing dry versus wet values of the interfacial fracture energy.

Figure 17, is a plot of the percent weight gain versus time for FP 4511 and 4450 when exposed to an atmosphere consisting of 85°C and 85% RH. After approximately 700 hours, FP 4511 gained close to .8 weight percent, whereas FP 4450 gained .4 weight percent.

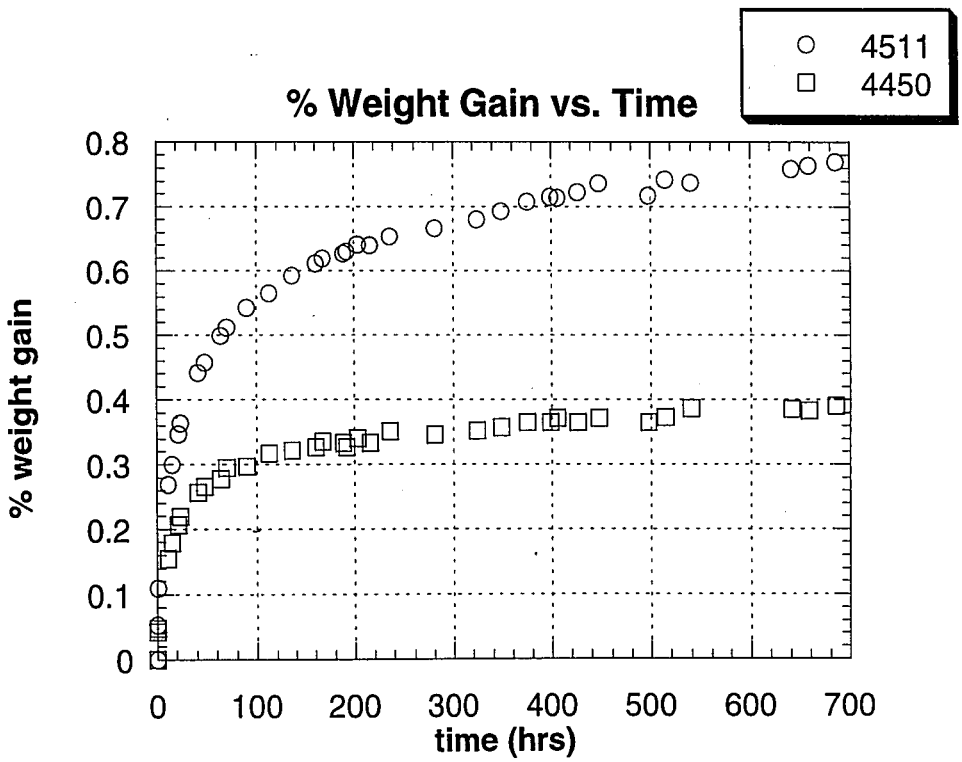

Figure 17. Percent weight gain versus time at 85°C/85% RH for FP 4450 and 4511.

Park et al.[35] have examined the humidity effects on adhesion strength between solder ball and epoxy underfills. Specifically, Hysol FP 4511 and Shin Etsu X-43-5235 underfills were studied. The authors subjected their specimens to an 85°C/85%RH environment and measured a decrease in the adhesive strength of the underfills with increasing exposure time. Park et al. also measured the water absorption of cured FP 4511 for 2 hours in a steam bomb (120°C, 2 atm.) and found that the FP 4511 absorbed 1.5 wt.% moisture as well as experienced a reduction in the glass transition temperature.

REFERENCES

1. A.A Griffith. Philos. Trans. R. Soc. London, Ser A 221, 163 (1920).
2. Richard Hertzberg. Deformation and Fracture Mechanics of Engineering Materials, John Wiley & Sons, 4th ed. 1996.
3. G.R. Irwin. Fracturing of Metals, ASM, Cleveland OH 1949, p147.
4. G.C.M. Sih. Handbook of Stress Intensity Factors, Lehigh University, Bethlehem, PA, 1973.
5. Richard Hertzberg. Deformation and Fracture Mechanics of Engineering Materials, John Wiley & Sons, 4th ed. 1996.
6. M. Charalambides, A.J. Kinloch, Y. Wang, and J.G. Williams. International Journal of Fracture, 54: (1992) 269-291.
7. J.W. Hutchinson and Z. Suo, Advances in Applied Mechanics 28 (1991).
8. J.R. Reeder and J.H. Crews. NASA Technical Memorandum 102777, January 1991.
9. J.R. Reeder and J.H. Crews. AIAA Journal, vol 28 no7. P1270-1276.
10. Peter Brandenburger. Mixed-Mode Fracture of Organic Chip Attachment Adhesives, M.S. Thesis, Lehigh University, 1995.
11. Malcolm Early. Manufacturing Systems Engineering M.S. Project, Lehigh University, 1996.

12. Luu Nguyen, Steven Gee, Martin Johnson, Herb Grimm, Hector Berardi, and Randy Walberg. IEEE Transactions on Components, Packaging, and Manufacturing Technology, Part A, vol 18, No 1, March 1995 15-21.

13. Luu Nguyen, Andrea Chen, and Randy Lo. EEP-Vol 11/MD-vol 64, Application of Fracture Mechanics in Electronic Packaging and Materials, ASME 1995. P35-44.

14. Young....need info on ref.

15. A.J. Kinloch. "Adhesion and Adhesives" Chapman and Hall, London, 1987.

16. R.J. Good. Contact Angle, Wetting and Adhesion: A Critical Review. K.L. Mittal (Editor), VSP Utrecht, The Netherlands, pp. 3-36, 1993.

17. Thomas Lloyd. Colloids and Surfaces A, 93 (1994) pp. 25-37.

18. A.J. Kinloch. Review The Science of Adhesion, Part 1 Surface and Interfacial Aspects, Journal of Mat Sci 15 (1980) 2141-2166.

19. A.G. Evans, M. Ruhle, B.J. Dalgleish, and P.G. Charalambides. Metallurgical Transactions A, Vol. 21A, September 1990. 2149-2429.

20. D. Maugis. Journal of Materials Science, 20 (1985) 3041-3073.

21. Jacques Schultz. J. Adhesion 1992, Vol. 37, pp 73-81.

22. Hamid Azimi and Raymond Pearson, and T.B. Lloyd. EEP-Vol 11/MD-Vol 64, Application of Fracture Mechanics in Electronic Packaging and Materials, ASME (1995) 155-161.

23. Siriwan Phattanarudee. Masters Thesis to be published at Lehigh University, Bethlehem, PA 1997.

24. A.J. Kinloch. Chimia 44 (1990), 318-321.

25. Luu Nguyen, Randall Walberg, and Charlie Chua. Advances in Electronic Packaging, ASME 1992. P751-762.

26. Y.H. Mei and S. Liu. EEP-Vol11/MD-Vol 64, Application of Fracture Mechanics in Electronic Packaging and Materials, ASME 1995. P 85-93.

27. Masazumi Amagai, Hideo Seno, and Kazuyoshi Ebe. IEEE Transactions on Components, Packaging, and Manufacturing Technology, Part B, Vol 18, No 1 February 1995. P119-125.

28. Seung-Ho Ahn and Young-Shin Kwon. IEEE Transactions on Components, Packaging, and Manufacturing Technology, Part B, Vol. 18, No 3, August 1995. P491-495.

29. A.A.O. Tay, G.L. Tan, and T.B. Lim. IEEE Transactions on Components, Packaging, and Manufacturing Technology, Part B: Advanced Packaging, Vol. 17 No 2, May 1994. P201-208.

30. Siriwan Phattanarudee. Paper presented at Techcon '96 in Phoenix, AZ.

31. Malcolm Early, Siriwan Phattanarudee, Ryan Hydro. Paper to be published.

32. A.N. Netravali, R.E. Fornes, R.D. Gilbert, and J.D. Memory. J. Appl. Polymer Sci., Vol. 29, 1984 p 311.

33. L. El-Sa'ad, M.I. Darby, and B. Yates. J. Materials Science 24, 1989, p 1653-1659.

34. Stephen Barton and Geoffrey Pritchard. Polymers for Advanced Technologies, Vol 5, 1993, p245-252.

35. C.E. Park, B.J. Han, and H.E. Bair. Polymer 38, 1997, p3811-3818.

VITA

Ryan Michael Hydro was born on March 2, 1973 in Allentown, PA to Ronald and Maryanne Hydro of Jim Thorpe, PA. Ryan grew up in Jim Thorpe and attended St. Joseph's School and then Marian Catholic High School in Hometown, PA. He then went on to college at Lehigh University in Bethlehem, PA and graduated with his B.S. in Materials Science and Engineering in June 1995. Upon graduation, Ryan pursued his M.S. in Materials Science and Engineering at Lehigh and graduated in December 1997.

END OF TITLE